JACS
JOURNAL OF THE AMERICAN CHEMICAL SOCIETY
Article
pubs.acs.org/JACS

Crystal Melting by Light: X-ray Crystal Structure Analysis of an Azo Crystal Showing Photoinduced Crystal-Melt Transition

Manabu Hoshino,*[,†,‡,⊥] Emi Uchida,[§] Yasuo Norikane,[§] Reiko Azumi,[§] Shunsuke Nozawa,[∥] Ayana Tomita,[∥] Tokushi Sato,[∥] Shin-ichi Adachi,[∥,#] and Shin-ya Koshihara[†,‡]

[†]Department of Chemistry and Materials Science, Tokyo Institute of Technology, Meguro-ku, Tokyo 152-8551, Japan
[‡]CREST, Japan Science and Technology Agency (JST), Chiyoda-ku, Tokyo 102-0076, Japan
[§]Electronics and Photonics Research Institute, National Institute of Advanced Industrial Science and Technology (AIST), Tsukuba, Ibaraki 305-8565, Japan
[∥]Photon Factory, High Energy Accelerator Research Organization, Tsukuba, Ibaraki 305-0801, Japan
[#]PRESTO, Japan Science and Technology Agency (JST), Chiyoda-ku, Tokyo 102-0076, Japan

Supporting Information

ABSTRACT: *Trans*−*cis* photoisomerization in an azo compound containing azobenzene chromophores and long alkyl chains leads to a photoinduced crystal-melt transition (PCMT). X-ray structure analysis of this crystal clarifies the characteristic coexistence of the structurally ordered chromophores through their $\pi\cdots\pi$ interactions and disordered alkyl chains around room temperature. These structural features reveal that the PCMT starts near the surface of the crystal and propagates into the depth, sacrificing the $\pi\cdots\pi$ interactions. A temporal change of the powder X-ray diffraction pattern under light irradiation and a two-component phase diagram allow qualitative analysis of the PCMT and the following reconstructive crystallization of the *cis* isomer as a function of product accumulation. This is the first structural characterization of a compound showing the PCMT, overcoming the low periodicity that makes X-ray crystal structure analysis difficult.

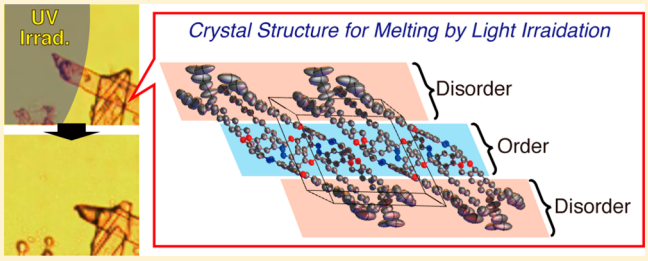

INTRODUCTION

Photoreaction in organic crystals is a valuable technique for synthetic chemistry because it is feasible for stereoselective and solvent-free reactions. Various kinds of photoreactions, such as dimerization, cyclization, and isomerization, proceed successfully in a solid state.[1,2] X-ray crystallography is an effective way to obtain an understanding of the mechanism of these photoreactions. Photodimerization of cinnamic acids in a crystalline phase was the first example of a reaction mechanism revealed by X-ray crystallography.[3] That and subsequent crystallographic work established the features of photochemical reactivity at a solid state: adjacency of reactants or reactive groups and limited motion of molecules in a solid phase.[2,4]

Recently, it was proposed that a photochemical phase transition accompanying a solid-state reaction must begin by formation of a solid solution (dilute mixed crystal of the product in the crystalline phase of the reactant) and ultimately reach either a same stable, a same metastable, a new stable, or an isotropic (melt or glass) phase of product.[2,5] The case of reaching a same stable phase is classified as a single crystal-to-single crystal reaction. In this type of reaction, initial, final, and possibly even intermediate phases in the reaction process can be directly observed by X-ray crystal structure analysis.[6,7] Reactions reaching a same metastable or new stable phase often lose long-range order in the initial crystalline phase, and it becomes increasingly difficult to track the reaction process by X-ray crystal structure analysis. In those cases, combining X-ray crystallography for the initial phase and spectroscopy and powder X-ray diffraction (PXRD) to track the phase change is effective in obtaining details about the reactions.[8−14] Crystals showing amorphization or melting by photoreaction have a tendency to become unsuitable for X-ray crystal structure analysis. It is difficult to obtain a suitable single crystal from recently reported solid-to-solid photoreactions that proceed via an amorphous[5] or a melt[15,16] phase, so discussions are based on PXRD, thermal analysis, spectroscopy, and observation with a microscope. Those data enable to researchers to reach a well-considered conclusion about the characterization of phases and macroscopic appearance of compounds during the reaction. However, to evaluate how solid solution sites are formed and macroscopically spread throughout a crystal during amorphization or melting, X-ray crystal structure analysis is required.

Herein, we describe the photochemical phase transition in an organic crystal reaching a melt phase (photoinduced crystal-melt transition, PCMT) on the basis of X-ray crystal structure analysis. An azobenzene derivative, azobenzenophane, in which two *trans*-azobenzene units with four dodecyloxy chain

Received: April 12, 2014
Published: June 11, 2014

   dx.doi.org/10.1021/ja503652c | J. Am. Chem. Soc. 2014, 136, 9158−9164

substituents are connected by methylene bridges (*trans*/*trans*-**1**, Figure 1a),[15,16] was selected as a target compound. The PCMT in *trans*/*trans*-**1**, observed using a microscope, is shown in Figure 1b,c and Supporting Video 1.

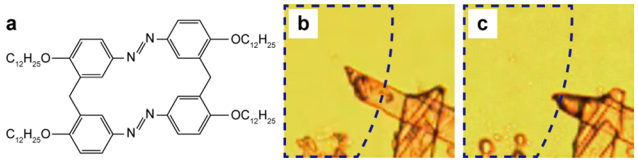

Figure 1. (a) Chemical structure of *trans*/*trans*-**1**. (b,c) Photographs of *trans*/*trans*-**1** on a microscope (b) before and (c) after 30 s of UV irradiation (UV-irradiated area is surrounded by a blue dashed line).

In a crystal of *trans*/*trans*-**1**, the azobenzene moiety is expected to have two important roles in the PCMT. One is the formation of structural order in the crystal via self-assembly of aromatic rings by $\pi\cdots\pi$ interactions. The other is a large geometric change caused by *trans*−*cis* photoisomerization, which results in the transition to a melt phase and sacrifices the $\pi\cdots\pi$ network. The long alkyl chains in *trans*/*trans*-**1** are expected to enhance the dynamic nature of molecules in a crystal.[16] However, their role in the PCMT has not been clarified. The thermal behavior of long alkyl chains can change the phase and properties of crystals[17] and is expected to enable the PCMT. In fact, *trans*−*cis* photoisomerization in crystals of some azobenzene derivatives only occurs near the surface,[18,19] and all reported azobenzene-based compounds showing the PCMT caused by *trans*−*cis* photoisomerization possess long-chain functional groups.[15,16,20]

The crystal structure of *trans*/*trans*-**1** should provide a rationale for *trans*−*cis* photoisomerization in a crystalline state and clarify the roles of azobenzene and alkyl chain moieties in the PCMT. However, clarification of the detailed crystal structure to describe its photomodulable character remains a formidable challenge because the reported PXRD pattern of *trans*/*trans*-**1** shows very low diffraction intensity, except for the lowest Bragg peak,[15] indicating that data with sufficient intensity for single-crystal X-ray structure analysis could not obtained under typical conditions. In this study, we successfully obtained the crystal structure of *trans*/*trans*-**1** using bright synchrotron X-rays and elucidated structural features governing the PCMT.

RESULTS AND DISCUSSION

Dynamic Nature of Alkyl Chains Due to the Thermal Effect. Single-crystal XRD was performed at beamline PF-AR NW14A in KEK, Japan. The experimental setup at this beamline has been reported elsewhere.[21,22] All crystal structures were solved by direct methods (SIR2011[23]) and refined using the full-matrix least-squares method (SHELXL-97[24]). Experimental details are described in the Supporting Information. To clarify the influence of the thermal behavior of long alkyl chains on the self-assembly of azobenzene groups in *trans*/*trans*-**1**, the temperature dependence of its crystal structure was examined. ORTEP diagrams of *trans*/*trans*-**1** at 90, 140, 190, 240, and 293 K are presented in Figure 2. All atomic displacement parameters (ADPs) in *trans*/*trans*-**1** increased with temperature. In particular, the ADPs around the termini of alkyl chains increased and geometric changes were observed in this region at 240 and 293 K. This shows that the disorder of alkyl chains induced by their thermal dynamic motion starts during heating

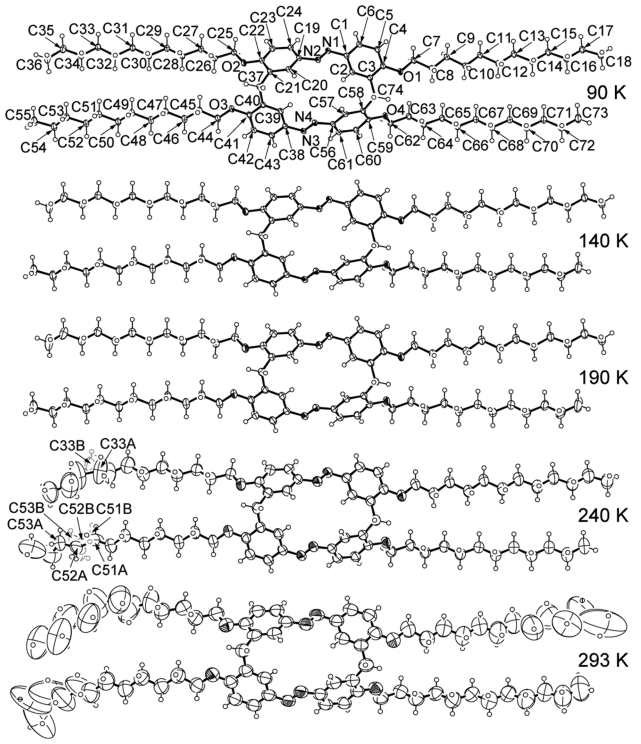

Figure 2. ORTEP diagrams of *trans*/*trans*-**1**, with thermal ellipsoids drawn at the 50% probability level and atom numbering shown, at 90, 140, 190, 240, and 293 K. Gray fragments at 240 K represent the disordered model obtained by structure analysis.

from 190 to 240 K, and becomes greater with increasing temperature. The thermal dynamic motion degrades molecular order in the crystal, especially in the regions containing alkyl chains. XRD intensities in the high-angle region decreased considerably with increasing temperature (Figure S1), confirming the degradation of order.[25] The ADPs and geometry of *trans*/*trans*-**1** were restored by cooling the crystal to 90 K (Figure S2).

The thermal effect on alkyl chains is evaluated in terms of their rigidity and size. Analysis of the ADPs by Hirshfeld's "rigid-bond" test[26] was used to describe rigidity of bonds in *trans*/*trans*-**1**. The differences of mean-square displacement amplitudes (ΔMSDA) along bond directions, utilized by the Hirshfeld test, at 90 and 293 K are summarized in Figure 3 (MSDAs at all temperatures are tabulated in Table S1). In the present work, a bond in which ΔMSDA is within 3 times its standard deviation is regarded as a rigid bond. All bonds in *trans*/*trans*-**1** are rigid at 90 K; however, at 293 K, many bonds lose rigidity, and ΔMSDAs around the termini of alkyl chains especially represent high conformational flexibility of those chains as a result of the thermal effect.

The sizes of alkyl chains at all temperatures are estimated by calculation of the Hirshfeld surface[27] of every alkyl chain using the program CrystalExplorer.[28] The volumes surrounded by the Hirshfeld surface of alkyl chains are tabulated in Table 1, and surface drawings at all temperatures are shown in Figure S3.The volumes around C9−C18 and C62−C73 gradually increased until reaching 190 K, and jumped at 240 and 293 K. The behaviors of the C25−C36 and C44−C55 chains differ from the others. The jump of the volume around the C25−C36 chain was seen at 293 K, and volume decrement above 240 K was shown on the C44−C55 chain. The reason for this

dx.doi.org/10.1021/ja503652c | J. Am. Chem. Soc. 2014, 136, 9158−9164

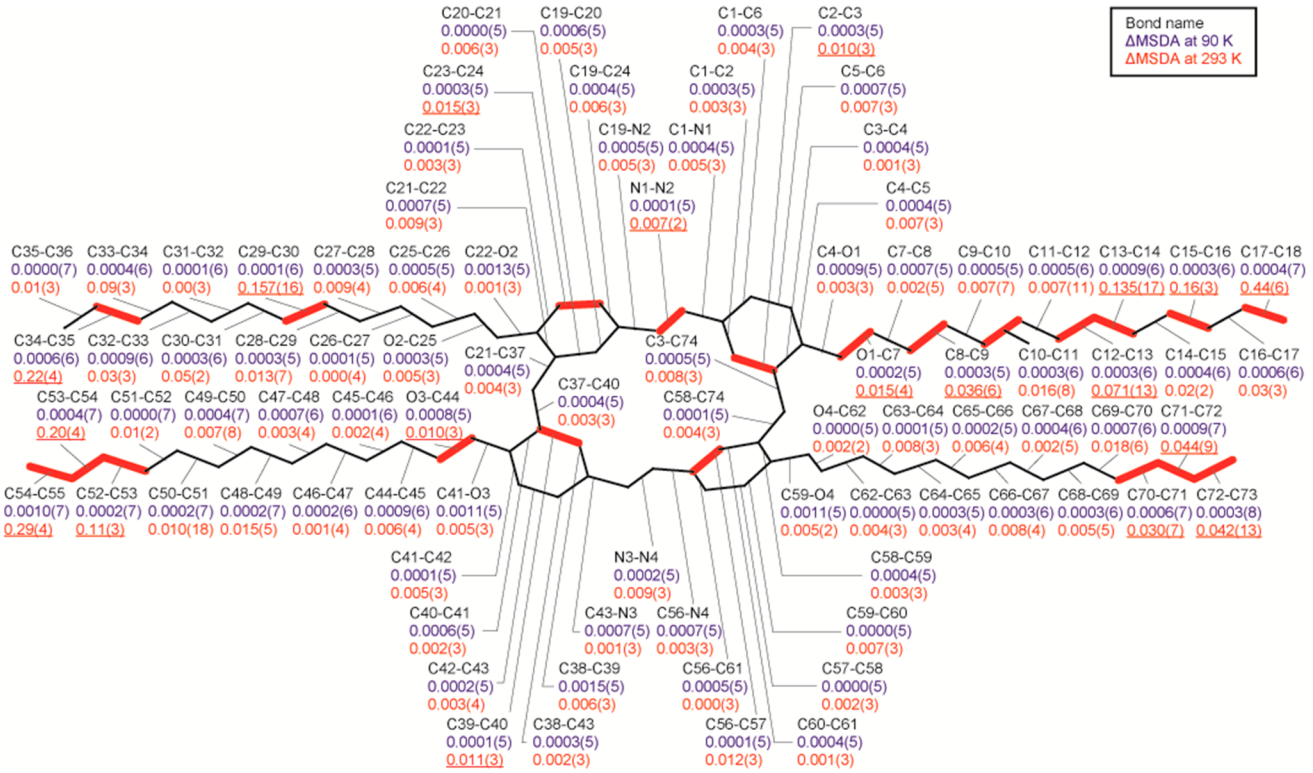

Figure 3. Differences of mean-square displacement amplitudes for all bonds in *trans/trans*-**1** at 90 (blue) and 293 K (red). The ΔMSDAs exceeding 3 times the standard deviation are underlined, and the corresponding bonds are shown by bold red lines.

Table 1. Volumes Surrounded by the Hirshfeld Surface of Alkyl Chains at Increasing Temperatures

temp/K	C9−C18/Å^3	C25−C36/Å^3	C44−C55/Å^3	C62−C73/Å^3
90	294.10	289.63	317.20	287.79
140	297.10	292.28	320.32	290.52
190	300.80	295.44	324.24	293.71
240	311.43	298.44	321.48	305.05
293	320.60	320.22	317.45	313.57

decrement is a large conformational change of the adjacent C25−C36 chain, which penetrates toward the C44−C55 chain above 240 K (Figure 2). An increment of the sum of the volumes around the C25−C36 and C44−C55 chains (619.68, 619.92, and 637.67 Å^3 at 190, 240, and 293 K, respectively) ensures a monotonic increase of the volume around their alkyl chains' sites with increasing temperature and a jump at 293 K.

Self-Assembling Nature of Azobenzene. The self-assembly of azobenzene in *trans/trans*-**1** can be evaluated by considering the diagrams of the packing motif of four selected molecules at different temperatures (Figure 4a). The dynamic thermal change of the crystal packing of *trans/trans*-**1** is shown in Supporting Video 2. The packing motif remained up to 190 K and then changed, accompanied by increasing disorder of the alkyl chains at 240 and 293 K. The self-assembly of azobenzene through weak intermolecular $\pi\cdots\pi$ interactions was also affected by the change in the packing motif. *trans/trans*-**1** contained $\pi\cdots\pi$ interactions between the offset-stacked (so-called parallel-displaced[29]) benzene rings: Ph1 (consisting of C19−24) or Ph2 (C56−61) and the ring related symmetrically by an inversion center (Figure 4a). The distances between vertical and horizontal centers of mass of two selected benzene rings (R1 and R2 in Figure 4b; values at 90, 140, 190, 240, and 293 K are presented in Table 2)[30,31] are used to evaluate $\pi\cdots\pi$ interactions. The distances R1 and R2 between Ph2's were ca. 3.7 and ca. 3.1 Å, respectively, at all temperatures. Such values indicate $\pi\cdots\pi$ interactions between these rings because substantial stabilization energies for similar R1 and R2 distances in theoretical calculations have been reported (1.394 kcal mol^{-1} for R1 = 3.6 Å and R2 = 3.5 Å; 1.205 kcal mol^{-1} for R1 = 4.0 Å and R2 = 3.0 Å).[31] In contrast, the distances between Ph1's showed a notable temperature dependence. The R2 distances between Ph1's are ca. 6 Å at lower temperatures (90, 140, and 190 K). Reported stabilization energies for parallel-displaced configurations indicate that the $\pi\cdots\pi$ interaction under such conditions is very weak (e.g., stabilization energies are 0.357 kcal mol^{-1} for R1 = 5.0 Å, R2 = 4.0 Å; 0.213 kcal mol^{-1} for R1 = 5.5 Å, R2 = 1.8 Å).[31] R2 became shorter by more than 2 Å with increasing temperature up to 293 K and became similar to the distance between Ph2's. This shortening indicates the formation of a relatively strong $\pi\cdots\pi$ interaction between Ph1's and a 1D network of azobenzenophanes involving these two kinds of $\pi\cdots\pi$ interactions around room temperature. This temperature dependence can be explained by considering the dynamic thermal motion of alkyl chains in terms of lattice energy minimization in the crystal. At lower temperature, because the dynamic motion of alkyl chains is thermally restricted, formation of numerous alkyl···alkyl and alkyl···π interactions is preferred over $\pi\cdots\pi$ interactions between Ph1's to minimize lattice energy. Conversely, at higher temperature, the thermal dynamic motion of alkyl chains prevents formation of these interactions. Instead, $\pi\cdots\pi$ interactions between Ph1's form, accompanied by reorganization of the packing motif to minimize the lattice energy at higher temperature. The shortest R2 between Ph2's at 240 K is considered as due to the alternative lattice energy minimization instead of insufficient

dx.doi.org/10.1021/ja503652c | J. Am. Chem. Soc. 2014, 136, 9158−9164

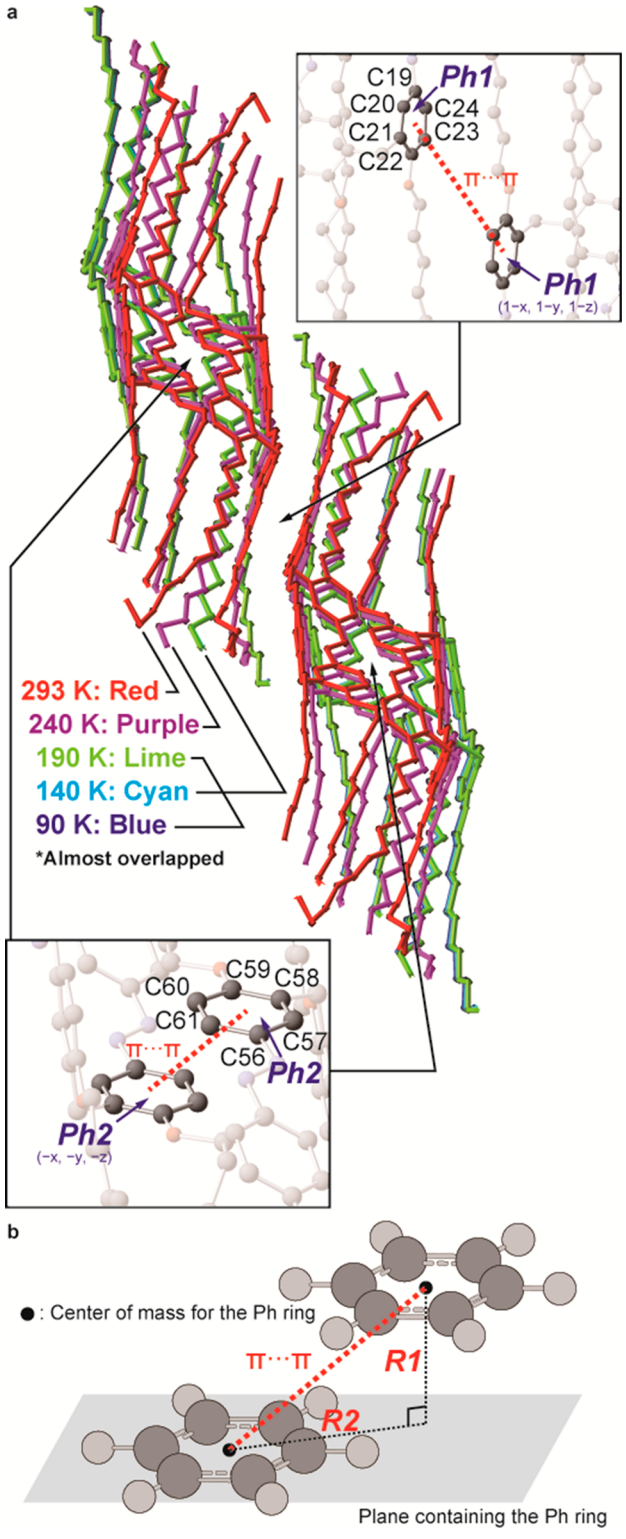

Figure 4. (a) Overlapping packing motif containing four molecules. The $\pi\cdots\pi$ interactions are shown by red dotted lines. (b) The definition of R1 and R2 used to evaluate the $\pi\cdots\pi$ interactions.

formation of $\pi\cdots\pi$ interactions between Ph1's at this temperature (R1 = 3.604 Å, R2 = 4.034 Å).

Recently, the $\sigma\cdots\sigma$ interaction between alkanes was investigated as significant for molecular stacking. Compared to the $\pi\cdots\pi$ interaction, the $\sigma\cdots\sigma$ interaction has similar stabilization energy and is more localized and directional.[32]

Table 2. Distances between Vertical (R1) and Horizontal (R2) Centers of Mass for Selected Two-Benzene Rings

	between Ph1's		between Ph2's	
temp/K	R1/Å	R2/Å	R1/Å	R2/Å
90	3.658	5.922	3.752	3.122
140	3.681	5.960	3.763	3.150
190	3.706	5.997	3.778	3.183
240	3.604	4.034	3.789	2.960
293	3.241	3.753	3.780	3.145

Reorganization of the packing motif by heating in the present study clearly shows that the $\sigma\cdots\sigma$ interactions between the alkyl chains at low temperatures reduce their mobility and contribute to the parallel arrangement of *trans/trans*-**1**. The prevention of interactions involving alkyl chains by their thermal motion at high temperatures is reflected in the localized and directional character of the $\sigma\cdots\sigma$ interaction.

Temperature-Dependent Responsivity of the PCMT. The responsivity of the PCMT of *trans/trans*-**1** depending on temperature was evaluated on the basis of the temporal change of its PXRD pattern around the strongest reflection (01−1; the 001 reflection for the lattice at 293 K, see Supporting Information) under UV irradiation (λ = 365 nm), as depicted in Figure 5. [Note that no reflections except for the strongest one could be collected with significant intensity because a polycrystalline thin-film sample was used for this measurement.] Experimental details are described in the Supporting Information, Figure S4. Generation of a Bragg peak at $2\theta \approx 2.1^\circ$ upon UV irradiation was found at 240 and 293 K. This new peak originates from the fully photoisomerized *cis/cis*-**1** crystallized from the photoinduced melt phase.[15] At 90, 140, and 190 K, on the other hand, the intensity of the 01−1 reflection decreased slightly, and no new peak was observed. This temperature dependence indicates that the crystal lattice change by thermal dynamic motion of alkyl chains and formation of the 1D network of $\pi\cdots\pi$ interactions between azobenzene moieties is required for the PCMT. The observed small decrease in the reflection intensity at 90, 140, and 190 K suggests partial amorphization due to the heterogeneous solid-state photoisomerization.[2] A heterogeneous solid-state reaction means preferential formation of product via a geometric change at defect sites and near the surface. The photochemical phase transition requires sufficient amounts of the solid solution site.[2,5] According to the reported geometry of *trans/trans*-**1**, *trans/trans*-[1,1]3,3′-azobenzenophane, and their isomers,[4,33] geometric change of *trans/trans*-**1** by *trans*−*cis* photoisomerization (even in partial photoisomerization from *trans/trans*-**1** to *trans/cis*-**1**) would be sterically prevented in the crystal,[34,35] and so an amorphous phase of photoproducts would form near the surface only. Some studies of *trans*−*cis* photoisomerization of azobenzene derivatives only near the surface have been reported, as an illustration.[18,19] This partial amorphization indicates that a sufficient amount of solid solution sites for the photochemical crystal−amorphous transition was formed by photoisomerization of *trans/trans*-**1** near the surface. An example of reconstructive crystal growth of a photoproduct from an amorphous phase during a photochemical phase transition process was reported elsewhere.[5] However, in the present work, no new Bragg peak generation was observed under the UV irradiation conditions at 90, 140, and 190 K. This indicates that the amount of solid solution sites of *cis/cis*-**1** in

dx.doi.org/10.1021/ja503652c | J. Am. Chem. Soc. 2014, 136, 9158−9164

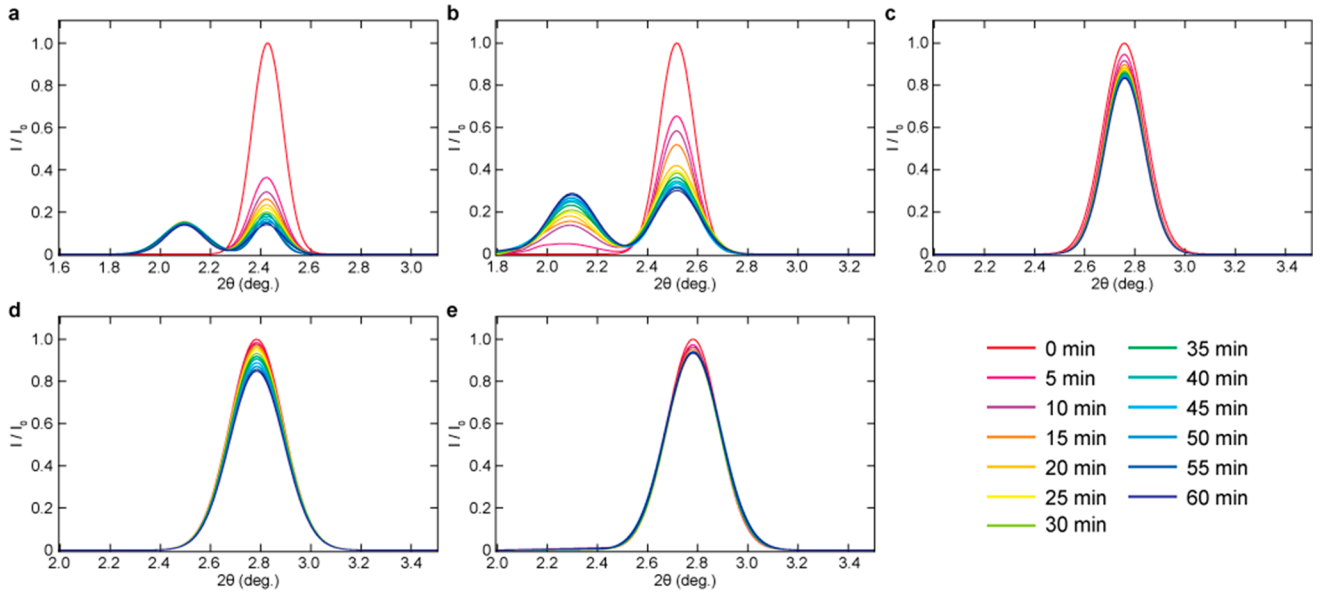

Figure 5. Photoinduced change of the powder XRD pattern of *trans*/*trans*-**1**. Temporal changes around the strongest Bragg peak at (a) 293, (b) 240, (c) 190, (d) 140, and (e) 90 K are shown. Diffraction data were recorded every 5 min for a total of 60 min after starting photoirradiation.

this partial amorphous phase is not enough for reconstruction of its crystals.

The same heterogeneous solid-state reaction is expected to occur at 240 and 293 K. In contrast to the lower temperature conditions, the PCMT occurred instead of amorphization near the surface only. At 240 and 293 K, the crystal lattice is mainly stabilized by the 1D network of $\pi\cdots\pi$ interactions between azobenzene moieties, because alkyl chains are barely ordered at those temperatures (as shown in Figures 2 and S1). When the 1D network of $\pi\cdots\pi$ interactions is sacrificed by photoisomerization of *trans*/*trans*-**1**, its structural order is entirely deteriorated, and the PCMT occurs. The slower temporal intensity decrement of the 01−1 (or 001) reflection and increment of the one corresponding to *cis*/*cis*-**1** at 240 K rather than at 293 K (see Figure 5a,b) indicates the shortest R2 between Ph2's (Table 2) and incomplete thermal size expansion of the C25−C36 and C44−C55 chains at 240 K (no jump yet in the heating process, Table 1). These results suggest that the stronger binding between Ph2's by the $\pi\cdots\pi$ interaction than at 293 K and the insufficient dynamic nature of the C25−C36 and C44−C55 chains reduce the reaction rate of *trans*−*cis* photoisomerization and the production rate of *cis*/*cis*-**1** for crystallization.

A similar loss of weak intermolecular interactions accompanied by *trans*−*cis* photoisomerization in another photoinduced macroscopic phenomenon, crystal bending, has been proposed to occur in other azobenzene derivatives.[8] In that case, mechanical stress-induced photoisomerization transforms a single crystal into polycrystals.[8,9] However, in the present case, thermal dynamic motion of long alkyl chains alters the role of the $\sigma\cdots\sigma$ interactions between them from stabilization of parallel ordering of *trans*/*trans*-**1** to increment of isotropic character at the regions containing alkyl chains in the crystal. This mitigates the mechanical stress accompanying photoisomerization and enables transformation to a completely disordered melt phase.

The temporal change of PXRD also indicates that the PCMT is not a thermal phenomenon. Simulated PXRD patterns based on the crystal structures obtained at the studied temperatures are shown in Figure 6a. The strongest reflection, used as an indicator for responsivity of the PCMT in the above discussion, showed a significant shift toward the low-angle region upon heating above 240 K (enlarged in Figure 6b). This shift is induced by lattice deformation due to thermal dynamic motion of alkyl chains (the interplanar distances associated with that reflection at 90 and 293 K are shown in Figure 6c,d). In contrast, the diffraction angle of that reflection under UV irradiation was maintained at the position before irradiation (PXRD at 0 min in Figure 5) at all temperatures, therefore showing that the effect of heating by light irradiation is negligible. Further, the transition temperatures of *trans*/*trans*-**1** are reported as 383 (crystal to liquid-crystal) and 418 K (liquid-crystal to melt),[15] which are substantially higher than the measurement temperatures in the present study. Those clearly indicate that the PCMT can be classified as a photochemical phase transition, characteristic of a photoinduced process.

Phase Characterization during the PCMT. On the basis of the results of the present study and the existing general model for photochemical phase transitions, a two-component phase diagram as a function of photoreaction progress[2,5] (shown in Figure 7) is applied for qualitative understanding of the PCMT. The melting points of *trans*/*trans*-**1** and *cis*/*cis*-**1** (at least 373 K[15]) are expressed as $T_{m(Reactant)}$ and $T_{m(Product)}$, respectively. Partial amorphization by UV irradiation at 90, 140, and 190 K indicates that the eutectic temperature (T_{Eut}) is between 190 and 240 K. The absence of the diffraction representing crystallization of *cis*/*cis*-**1** from the amorphous phase indicates that the accumulation of *cis*/*cis*-**1** near the surface was not enough for the reaction to progress at the amorphous−PLP line in the diagram.

At 240 and 293 K, the PCMT and generation of the new Bragg peak indicate that the reaction progressed at the PLP + liquid region. Partial melting near the surface propagates into the depth of the crystal using the solid−liquid interface, and so the PCMT was undergone with high conversion. However, the reaction could not progress to the PLP region because the generated *cis*/*cis*-**1** absorbs and attenuates the excitation light,[15,16] preventing sufficient accumulation of *cis*/*cis*-**1** in

dx.doi.org/10.1021/ja503652c | J. Am. Chem. Soc. 2014, 136, 9158−9164

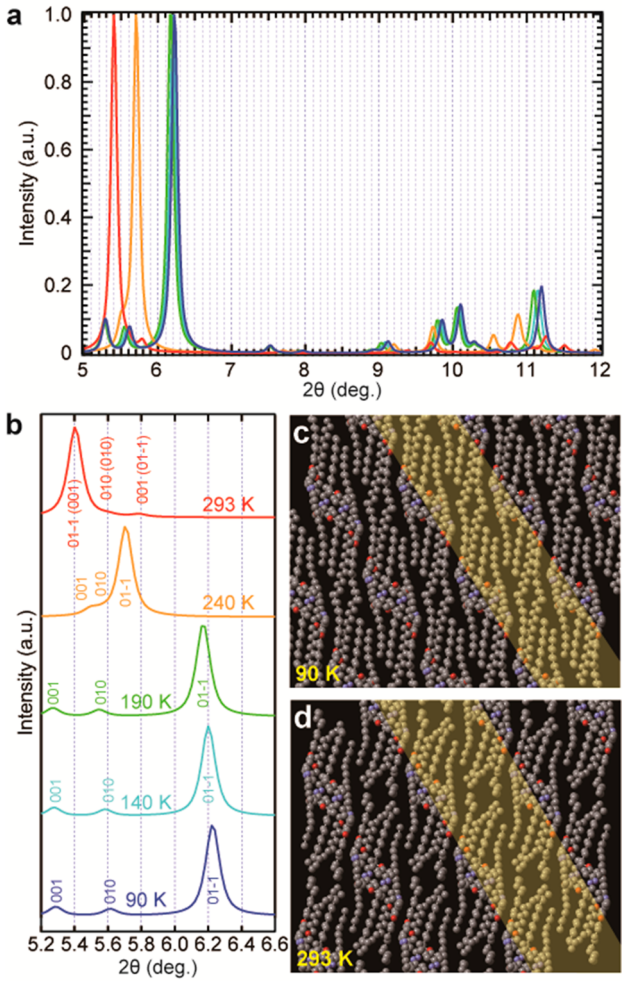

Figure 6. Temperature dependences of PXRD and the interplanar distance in *trans/trans*-**1**. Simulated PXRD patterns at all measured temperature are in the ranges (a) 5° < 2θ < 12° and (b) 5.2° < 2θ < 6.6°. The interplanar distances correspond to the 01−1 (yellow area, 001 at 293 K) reflections at (c) 90 and (d) 293 K.

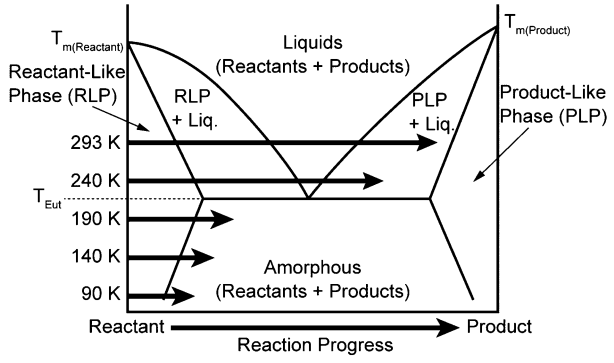

Figure 7. Two-component phase diagram for the PCMT of *trans/trans*-**1**. Reactant-like (product-like) phase is a solid solution containing the products (reactants) in the crystalline phase of the reactant (product). The arrows in the diagram represent reaction progress in the present study.

that region.[36] In fact, the residual 01−1 (or 001) reflection, having ca. 15% of the initial intensity, similar to the reported sum of ratios of *trans/trans*-**1** and *trans/cis*-**1** (ca. 20%) in the thin-film condition at a photostationary state,[15] after 60 min of UV irradiation suggested that ca. 15% of the phase remained as the RLP. This attenuation effect was reflected in a gradual decrement of the initial diffraction intensity, despite a constant diffraction intensity corresponding to *cis/cis*-**1** since 5 min after the start of UV irradiation at 293 K (Figure 5a). The generated *cis/cis*-**1** attenuated the excitation light, and so not enough photons to progress the reaction to the PLP + liquid region could reach the solid−liquid interface. As a result, after 60 min of UV irradiation, the crystal is considered to show a phase gradient (shown schematically in Figure 8).

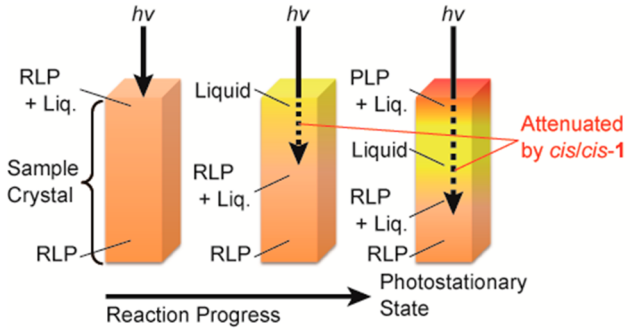

Figure 8. Schematic drawing representing a phase gradient expected in the PCMT process of *trans/trans*-**1**.

CONCLUSIONS

The detailed structural features governing the PCMT of *trans/trans*-**1** can be determined by single-crystal X-ray structure analysis. In *trans/trans*-**1**, structural order (the 1D $\pi\cdots\pi$ network of azobenzene moieties) and disorder (dynamically moved long alkyl chains) coexist. The crystal structure and expected geometry of isomers represent photoisomerization of *trans/trans*-**1** to form a solid solution as a precursor to the PCMT near the surface at the beginning and a solid−liquid interface during its propagation into the depth of the crystal. In case of the reported well-ordered azobenzene-based crystals[7,8] and the lower temperature conditions of the present study, *trans*−*cis* photoisomerization of azobenzene occurs only near the surface, and as a result, transformation from a single crystal to polycrystals[19] or partial amorphization is shown instead of the PCMT. However, the coexistence of order and disorder in *trans/trans*-**1** around room temperature reported herein indicates that the PCMT occurs as a consequence of *trans*−*cis* photoisomerization of azobenzene moieties, involving loss of the 1D order of the $\pi\cdots\pi$ network as expected and formation of an entirely disordered isotropic phase of photoproducts with the assistance of disordered alkyl chains. Along with this assistance, the thermal behavior of the long alkyl chains also affects the formation of the structure with coexisting order and disorder. The $\sigma\cdots\sigma$ interactions between alkyl chains contribute to the close parallel ordering of *trans/trans*-**1** in the crystal at low temperatures. However, the thermal dynamic motion of the chains prevents formation of alkyl···alkyl and alkyl···π interactions, and encourages interaction of the 1D $\pi\cdots\pi$ network of azobenzene groups by self-assembly of their aromatic rings around room temperature as a prerequisite for the PCMT. Application of the two-component phase diagram to the present study generalizes the PCMT as a function of accumulation of photoproduct. The difference in photochemical phase transition at the higher temperatures (240 and 293 K, showing the PCMT) and lower temperatures (90,

dx.doi.org/10.1021/ja503652c | J. Am. Chem. Soc. 2014, 136, 9158−9164

140, and 190 K, showing the partial amorphization) can be clearly classified on the basis of accumulation of *cis*/*cis*-**1**. Our insights will contribute to enhancing the general understanding about photochemical phase transitions, especially transitions reaching an isotropic phase, which should be valuable in the design of photofunctional materials and the development of selective and solvent-free synthesis by photoreactions at a solid state.

■ ASSOCIATED CONTENT

Supporting Information

Experimental details, supporting data and figures, crystallographic information file (CIF), and supporting videos 1 (file ja503652c_si_003.mov) and 2 (file ja503652c_si_004.mov). This material is available free of charge via the Internet at http://pubs.acs.org.

■ AUTHOR INFORMATION

Corresponding Author

mhoshino@appchem.t.u-tokyo.ac.jp

Present Address

[⊥]M.H.: Department of Applied Chemistry, The University of Tokyo, 7-3-1 Hongo, Bunkyo-ku, Tokyo 113-8656, Japan

Notes

The authors declare no competing financial interest.

■ ACKNOWLEDGMENTS

This work was approved by the Photon Factory Program Advisory Committee (PF-PAC Nos. 2009S2-001, 2009G626, and 2011G591). Y.N. thanks JSPS KAKENHI (21750157, 23760680), the Association for the Progress of New Chemistry, Iketani Science and Technology Foundation, and The Canon Foundation.

■ REFERENCES

(1) Kaupp, G. *Top. Curr. Chem.* **2005**, *254*, 95−183.
(2) Keating, A. E.; Garcia-Garibay, M. A. Photochemical Solid-to-Solid Reactions. In *Organic and Inorganic Photochemistry*; Ramamurthy, V., Schanze, K., Eds.; Marcel Dekker: New York, 1998; Vol. 2, pp 195−248.
(3) (a) Cohen, M. D.; Schmidt, G. M. J. *J. Chem. Soc.* **1964**, 1996−2000. (b) Cohen, M. D.; Schmidt, G. M. J.; Sonntag, F. I. *J. Chem. Soc.* **1964**, 2000−2013. (c) Schmidt, G. M. J. *J. Chem. Soc.* **1964**, 2014−2021.
(4) Ramamurthy, V.; Venkatesan, K. *Chem. Rev.* **1987**, *87*, 433−481.
(5) de Loeroa, D.; Stopin, A.; Garcia-Garibay, M. A. *J. Am. Chem. Soc.* **2013**, *135*, 6626−6632.
(6) Ohashi, Y. *Chem. Rec.* **2013**, *13*, 303−325.
(7) Ohashi, Y. *Crystallogr. Rev.* **2013**, *19* (Suppl. 1), 2−146.
(8) Bushuyev, O. S.; Tomberg, A.; Friščić, T.; Barrett, C. J. *J. Am. Chem. Soc.* **2013**, *135*, 12556−12559.
(9) Naumov, P.; Sahoo, S. C.; Zakharov, B. A.; Boldyreva, E. V. *Angew. Chem., Int. Ed.* **2013**, *52*, 9990−9995.
(10) Salzillo, T.; Bilotti, I.; Della Valle, R. G.; Venuti, E.; Brillante, A. *J. Am. Chem. Soc.* **2012**, *134*, 17671−17679.
(11) de Loera, D.; Garcia-Garibay, M. A. *Org. Lett.* **2012**, *14*, 3874−3877.
(12) Lee, J. H.; Naumov, P.; Chung, I. H.; Lee, S. C. *J. Phys. Chem. A* **2011**, *115*, 10087−10096.
(13) Naumov, P.; Sakurai, K. *Cryst. Growth. Des.* **2005**, *5*, 1699−1701.
(14) Choi, T.; Cizmeciyan, D.; Kahn, S. I.; Garcia-Garibay, M. A. *J. Am. Chem. Soc.* **1995**, *117*, 12893−12894.
(15) Uchida, E.; Sakaki, K.; Nakamura, Y.; Azumi, R.; Hirai, Y.; Akiyama, H.; Yoshida, M.; Norikane, Y. *Chem.—Eur. J.* **2013**, *19*, 17391−17397.
(16) Norikane, Y.; Hirai, Y.; Yoshida, M. *Chem. Commun.* **2011**, *47*, 1770−1772.
(17) Cabus, S.; Bogaerts, K.; Mechelen, J. V.; Smet, M.; Goderis, B. *Cryst. Growth Des.* **2013**, *13*, 3438−3446.
(18) Bushuyev, O. S.; Singleton, T. A.; Barrett, C. J. *Adv. Mater.* **2013**, *25*, 1796−1800.
(19) Koshima, H.; Ojima, N.; Uchimoto, H. *J. Am. Chem. Soc.* **2009**, *131*, 6890−6891.
(20) Okui, Y.; Han, M. *Chem. Commun.* **2012**, *48*, 11763−11765.
(21) Hoshino, M.; Nozawa, S.; Sato, T.; Tomita, A.; Adachi, S.; Koshihara, S. *RSC Adv.* **2013**, *3*, 16313−16317.
(22) Hoshino, M.; Uekusa, H.; Tomita, A.; Koshihara, S.; Sato, T.; Nozawa, S.; Adachi, S.; Ohkubo, K.; Kotani, H.; Fukuzumi, S. *J. Am. Chem. Soc.* **2012**, *134*, 4569−4572.
(23) Burla, M. C.; Caliandro, R.; Camalli, M.; Carrozzini, B.; Cascarano, L.; Giacovazzo, C.; Mallamo, M.; Mazzone, A.; Polidori, G.; Spagna, R. *J. Appl. Crystallogr.* **2012**, *45*, 357−361.
(24) Sheldrick, G. M. *Acta Crystallogr. A* **2008**, *64*, 112−122.
(25) Watkin, D. J. *Crystal Structure Analysis: Principles and Practice*, 2nd ed.; Oxford University Press: New York, 2009; pp 169−185.
(26) Hirshfeld, F. L. *Acta Crystallogr., Sect. A* **1976**, *32*, 239−244.
(27) Spackman, M. A.; Jayatilaka, D. *CrystEngComm* **2009**, *11*, 19−32.
(28) Wolff, S. K.; Grimwood, D. J.; McKinnon, J. J.; Turner, M. J.; Jayatilaka, D.; Spackman, M. A. *CrystalExplorer*, Version 3.1; University of Western Australia: Crawley, 2012.
(29) Riley, K. E.; Hobza, P. *Acc. Chem. Res.* **2013**, *46*, 927−936.
(30) Sinnokrot, M. O.; Valeev, E. F.; Sherrill, C. D. *J. Am. Chem. Soc.* **2002**, *124*, 10887−10893.
(31) Hobza, P.; Selzle, H. L.; Schlag, E. W. *J. Phys. Chem.* **1996**, *100*, 18790−18794.
(32) Alonso, M.; Woller, T.; Martín-Martínez, F. J.; Contreras-García, J.; Geerlings, P.; De Proft, F. *Chem.—Eur. J.* **2014**, *20*, 4931−4941.
(33) Norikane, Y.; Kitamoto, K.; Tamaoki, N. *J. Org. Chem.* **2003**, *68*, 8291−8304.
(34) Sworakowski, J.; Janus, K.; Nešpůrek, S. *Adv. Colloid Interface Sci.* **2005**, *116*, 97−110.
(35) Tsuda, M.; Kuratani, K. *Bull. Chem. Soc. Jpn.* **1964**, *37*, 1284−1288.
(36) Enkelmann, V.; Wegner, G.; Novak, K.; Wagener, K. B. *J. Am. Chem. Soc.* **1993**, *115*, 10390−10391.